Cell and Tissue Research (2023) 391:375–391
https://doi.org/10.1007/s00441-022-03706-w

REGULAR ARTICLE

Effects of bepridil on early cardiac development of zebrafish

Ya-Lan Wei[1,2,3] · Yu-Qing Lei[1,2] · Zhou-Jie Ye[1,2,3] · Xu-Dong Zhuang[1,2,3] · Li-Ping Zhu[1,2,3] · Xin-Rui Wang[1,2,3] · Hua Cao[1,2,3]

Received: 2 March 2022 / Accepted: 6 November 2022 / Published online: 23 November 2022

Abstract

Bepridil is a commonly used medication for arrhythmia and heart failure. It primarily exerts hemodynamic effects by inhibiting Na^+/K^+ movement and regulating the Na^+/Ca^{2+} exchange. In comparison to other Ca^{2+} inhibitors, bepridil has a long half-life and a complex pharmacology. Additionally, it is widely used in antiviral research and the treatment of various diseases. However, the toxicity of this compound and its other possible effects on embryonic development are unknown. In this study, we investigated the toxicity of bepridil on rat myocardial H9c2 cells. After treatment with bepridil, the cells became overloaded with Ca^{2+} and entered a state of cytoplasmic vacuolization and nuclear abnormality. Bepridil treatment resulted in several morphological abnormalities in zebrafish embryo models, including pericardium enlargement, yolk sac swelling, and growth stunting. The hemodynamic effects on fetal development resulted in abnormal cardiovascular circulation and myocardial weakness. After inhibiting the Ca^{2+} transmembrane, the liver of zebrafish larvae also displayed an ectopic and deficient spatial location. Additionally, the results of the RNA-seq analysis revealed the detailed gene expression profiles and metabolic responses to bepridil treatment in zebrafish embryonic development. Taken together, our study provides an important evaluation of antiarrhythmic agents for clinical use in prenatal heart patients.

Keywords Bepridil · Cardiac development · Cardiotoxicity · Oxidative stress · Apoptosis

Introduction

With an average prevalence of nearly 25%, atrial fibrillation can easily precipitate the development of heart failure. By 2030, the patient population will have increased by 46% (Carlisle et al. 2019). As a result, it is critical to strengthen cardiovascular therapeutic drug research, supervision, and toxicity assessment (Pettit et al. 2010).

Bepridil belongs to the class IV antiarrhythmic agents and mainly treats cardiovascular disorders. The effects of bepridil treatment include regulation of the Na^+/Ca^{2+} exchange and the Na^+/K^+ movement (Zeller and Spinler 1987). In comparison to other calcium channel inhibitors, bepridil has a prolonged antigenic effect. Bepridil has a 42-h half-life and is effective for the dilatation of coronary vessels. As a result, it is considered an effective medication for long-term sinus rhythm maintenance in patients with atrial fibrillation or atrial flutter (Zeller and Spinler 1987; Aizawa et al. 2013). However, the precise mechanisms by which bepridil induces supraventricular or ventricular tachycardias remain unknown. A few cases indicate its efficacy in arrhythmias, which contributes to the controversy surrounding bepridil's use in the treatment of cardiovascular disease (Yedinak 1993).

In the last three decades, research on bepridil's effects has primarily focused on three aspects. To begin with, bepridil treatment resulted in a prolongation of the QT interval (Hollingshead et al. 1992). Several cases were reported where

Ya-Lan Wei and Yu-Qing Lei have contributed equally to this work and share the first authorship.

✉ Xin-Rui Wang
wanxiru@sjtu.edu.cn

✉ Hua Cao
caohua69@fjmu.edu.cn

[1] NHC Key Laboratory of Technical Evaluation of Fertility Regulation for Non-Human Primate, Fujian Maternity and Child Health Hospital, Fuzhou, Fujian 350013, China

[2] College of Clinical Medicine for Obstetrics & Gynecology and Pediatrics, Fujian Medical University, Fuzhou, Fujian 350122, China

[3] Medical Research Center, Fujian Maternity and Child Health Hospital, Fuzhou, Fujian 350001, China

bepridil exacerbated cardiac arrhythmias and their association with torsade de pointes (Hasegawa 1988). Bepridil's primary efficacy in treating arrhythmias is due to its hemodynamic effects, which decrease myocardial contraction and heart rate while increasing coronary blood flow. These physiological changes are ultimately intended to decrease myocardial oxygen consumption (Zeller and Spinler 1987). Thus, patients must closely monitor physiological parameters such as hypokalemia prior to taking bepridil (Hollingshead et al. 1992). Candesartan and bepridil were recently combined to overcome insufficient SR maintenance and QT prolongation (Kawamura et al. 2013). In several patients, the QT prolongation caused by bepridil treatment was also within the safe range (Aizawa et al. 2013). Continuous monitoring of the patient's serum concentration and ECG during medication may also help avoid the adverse effect of excessive QT prolongation (Wang et al. 2021). Bepridil is still effective in maintaining sinus rhythm in patients with refractory atrial fibrillation (Nishino et al. 2013).

Secondly, the short- and long-term treatments of bepridil had distinct effects on cardiomyocytes. For instance, bepridil blocks many cardiac ion channels, including the Na + channel current (*I*Na), in a dose-dependent manner (Sato et al. 1996). In contrast, bepridil dose dependently inhibits a variety of cardiac ion channels, including the Na^+ channel current (*I*Na) (Sato et al. 1996). On the other hand, long-term treatment with bepridil inhibited calmodulin action and increased *I*Na (Kang et al. 2009). Bepridil completely or partially blocks Na^+-dependent Ca^{2+} efflux during Na^+-Ca^{2+} exchange (Garcia et al. 1988). Because bepridil's toxicity is unknown, the majority of clinical studies lack long-term medication reports. We hypothesized that Ca^{2+} accumulation in the mitochondria of myocardial cells might result in cell death following long-term bepridil treatment (Tari et al. 1987). Additionally, an excess of intracellular Ca^{2+} may impair calmodulin activity and the ubiquitin–proteasome system (Kang et al. 2009).

The third point is highlighted in the complex pharmacologic profile of bepridil (Zeller and Spinler 1987). Bepridil also functions in exercise-induced myocardial ischemia and angina pectoris. The clinical experimental results, on the other hand, revealed dizziness, liver dysfunction, and even death cases (Hill et al. 1985). The most typical event is multiple patients resulting in bepridil-induced pulmonary toxicity, which directly led to the suspension of bepridil in the USA (Gaku et al. 2003; Suzuki et al. 2009; Watanabe et al. 2009).

While bepridil carries a risk of interstitial pneumonia, steroid therapy can help alleviate it (Yamase et al. 2012). As a result, bepridil is still widely used in many countries as a Ca^{2+} channel blocker for cardiovascular disorders. On the contrary, bepridil has been used in research on a variety of diseases due to its complex pharmacology. At present, it is primarily used to inhibit viruses. Although there is no definitive treatment for filovirus infections, bepridil inhibits the Ebola and Marburg viruses and significantly increases the survival rate of infected mice (DeWald et al. 2018; Ren et al. 2018). Additionally, numerous studies have demonstrated that bepridil has antiviral activity against coronavirus at low micromolar effective concentrations (Vatansever et al. 2021). Additionally, bepridil inhibits leukemic cell infiltration via regulation of the NOTCH1 pathway and induces cell apoptosis (Baldoni et al. 2018). Tsubota et al. (2021) described a novel effect of bepridil on colonic hypersensitivity and anticipated its application in the treatment of visual pain. Additionally, bepridil is an alkalescent reagent that inhibits both beta- and gamma-secretase generation in primary neurons of mice. It enables the development of dual-targeted amyloid precursor protein drugs (Mitterreiter et al. 2010).

Gestational heart disease and hypertension bring more significant risks and challenges to fetal pregnancy. Patients with hypertension and arrhythmia can take Ca^{2+} blocking agents appropriately under the instruction of drug toxicity assessment during early pregnancy (Ramlakhan et al. 2020). Bepridil is able to pass through the placenta and is excreted in human milk (unpublished data on file, Organon). However, the embryotoxicity of bepridil has not been evaluated in terms of fetal fate. Animal embryo models are frequently used to assess embryotoxicity (van Veenendaal et al. 2013). In humans and zebrafish (*Danio rerio*), drug-induced QT prolongation is extremely conservative, resulting in bradycardia and AV blockade (Milan et al. 2003).

In this study, we verified the effects of bepridil on cardiomyocyte proliferation and embryonic development in in vitro rat myocardial cells and transgenic zebrafish embryos. We demonstrated the defective growth of cardiac and liver progenitor cells during cardiomyocyte migration and organic metabolism. Additionally, we sequenced the gene expression profiles of zebrafish larvae following treatment with various concentrations of bepridil.

Methods

Zebrafish husbandry and embryo collection

The wild-type (AB strain) zebrafish, *Tg (myl7:eGFP)* and *Tg (fabp10a:dsRed)* transgenic lines were purchased from the China Zebrafish Resource Center (http://www.zfish.cn/). Adult male and female zebrafish were maintained separately at 28 ± 1 ℃ under the 14-h light/10-h dark cycles. For fertilization, the adult zebrafish were mated in a ratio of 2:1 male to female. Then, the healthy and fertilized eggs were selected using a light microscope (Nikon, SMZ800N). The embryos were randomly divided into several groups and maintained in standard E3 medium (5 mM NaCl, 0.17 mM

KCl, 0.33 mM $MgSO_4$, and 0.33 mM $CaCl_2$) in a constant 28 ℃ incubator. The cultured embryos were replaced with fresh E3 medium every day, and the dead embryo was removed. All zebrafish experiments were performed following the guidance and administration of the Animal Research Committee at Fujian Maternity and Child Health Hospital (License No. 2021KLRD649).

Embryo handling and drug treatment

The bepridil hydrochloride ($C_{24}H_{34}N_2O$·HCl, Cat. 74,764–40-2, molecular weight: 403, purity ≥ 98%) was purchased from Sigma-Aldrich (Cat. B5016) and dissolved in sterilized ddH_2O to 2 mg/mL for storage.

Healthy zebrafish embryos at 24 hpf were selected under a light microscope (Nikon, SMZ800N) and transferred into the 6-well plates. Each experiment was duplicated three times and contained 15 individuals. The embryos were exposed to different concentrations of bepridil (250, 750, 1000, 1125, 1250, 1375, 1500, 2000, and 3000 ng/mL), which were diluted in the E3 medium. And the standard E3 medium was used as the control group.

We recorded the numbers of dead and malformed individuals at 48 hpf, 72 hpf, 96 hpf, and 120 hpf. The semi-lethal concentration (LC_{50}) and LC_{10} of bepridil for zebrafish larvae at 120 hpf were estimated to be 2123.59 and 1295 ng/mL using GraphPad software (GraphPad Prism 8.0.1). Accordingly, we selected a gradient treatment of bepridil of 250, 750, and 1295 ng/mL for embryotoxic assessment.

Cell culture and drug treatment

Rat myocardial cells H9c2 (ATCC, CRL-1446) were cultured in the DMEM medium (Gibco, Cat. C11995500BT) containing 10% fetal bovine serum (Hyclone, Cat.SV30208.02) in a humidified incubator (Thermo Scientific, 3131) with 5% CO_2 at 37 ℃. The cells were cultured typically until 60% cell confluence. Then, the culturing medium was discarded and the cells were rinsed twice with 0.01-M phosphate-buffered saline (PBS, Hyclone, Cat.SH30256.01) twice. The bepridil was diluted with the complete culture medium at the final concentrations of 0, 7, 15, 22, 30, 37, 45, and 52 μM.

For the Cell Counting Kit-8 (CCK-8) assay, the cells were treated with bepridil for 24 h. The culturing medium was replaced with the serum-free DMEM medium and 100 μL CCK-8 (Dojindo, Cat. CK04) in each well. Then, the cells were incubated for another 1.5 h in the incubator at 37 ℃. The values of the excitation waves were recorded at OD_{450} nm. The viability IC_{50} of bepridil treatment for H9c2 cells was estimated at 27 μM by GraphPad software. Afterwards, the concentrations of 0, 30, and 35 μM of bepridil were selected for subsequent experiments.

Morphological analyses

Zebrafish larvae at 120 hpf in each group were anesthetized with 0.02% tricaine methanesulfonate (Sigma-Aldrich, Cat. E10521) and mounted on a 15-mm glass bottom cell culture dish (Nest, Cat.801002) in 3% methylcellulose (Sangon, Cat. A600616). The morphological images of the whole larvae were observed and captured by a stereomicroscope (Leica, S9i). The body length, area of the yolk sac, hepatic fluorescence area, cardiac fluorescence area, pericardial area (PA), and the distance of sinus venous to bulbous arteriosus (SV-BA) were measured through the ImageJ software (ImageJ, 1.53c).

Microscopy and time-lapse imaging

The cardiac and hepatic morphological images, as well as the corresponding bright-field images (Figs. 4h–h''', 7a-a''') of *Tg (myl7:eGFP)* and *Tg (fabp10a:dsRed)* zebrafish were taken using a Leica light microscope (Leica, DM2500), which equipped with a 10 × /0.25 objective and a Leica MC170HD digital camera. The high-resolution fluorescence images, three-dimension images, and time-lapse imaging of zebrafish larvae were collected with a laser scanning confocal microscope (Leica, TCS SP8) with a 10 × /0.40 objective. The anesthetic zebrafish larvae were mounted with 3% methylcellulose. For alive larva imaging, the specimen was maintained at 10 ℃ for 2 min to slow down the heartbeat. Confocal imaging acquired z-stacks by a step size of 5 μm up to 200 μm depth in the heart and 5 up to 160 μm depth in the liver.

Acridine orange (AO) staining

The apoptotic cells of 120 hpf zebrafish larvae were detected by an AO assay (Sangon Biotech, Cat. E607307). The larvae were fixed with 4% paraformaldehyde (PFA) overnight. After washing with pre-cooling PBS, each sample was supplied with 1-mL AO staining solution according to the manufacturer's instructions at room temperature for 30 min. The images were collected with a laser scanning confocal microscope (Leica, TCS SP8) with 10 × /0.40 objectives.

Reactive oxygen species (ROS) assay

The ROS assay (Beyotime, Cat. S0033S) was used to detect oxidative stress levels after bepridil treatment. The larvae and H9c2 cells were fixed with 4% PFA overnight and rinsed with pre-cooling PBS. Each sample was incubated with 10 μM DCFH-DA (diluted with serum-free DMEM) at 37 ℃ for 30 min. The positive control of each group was added with 10 μM Rosup according to the manufacturer's

instruction. The images of larvae were photographed with a laser scanning confocal microscope (Leica, TCS SP8) with a 10×/0.40 objective. The ROS of H9c2 cells was assessed by flow cytometry using a flow cytometer (BD LSRFortessa™ Cell Analyzer, Cat. 647,800) with an excitation wavelength of 488 nm.

Giemsa staining

The adherent cells were fixed with 70% ethanol for 10 min and rinsed with sterilized ddH_2O 5 min three times for morphological imaging. Then, the cells were stained with Giemsa (Beyotime, Cat. C0131) for 1 h. The cells were washed with sterilized ddH_2O and collected using an inverted microscope (Nikon Eclipse TSZR) with 10×/0.30, 20×/0.45 objectives.

Cell cycle and apoptosis analyses

For cell cycle analyses, the cells in each group were harvested by 0.25% trypsin EDTA (BasalMedia, Cat. S310KJ) and rinsed with pre-cooling PBS. The cells were fixed with 70% ethanol for 12 h at 4 ℃. After washing with PBS three times, the cells were incubated with propidium (PI) staining solution (Beyotime, Cat. C1052) at 37 ℃ for 30 min.

The suspended cells were harvested and washed as described for PI staining for cell apoptosis analyses. Then, the cells were incubated with binding buffer, annexin V-FITC, and PI staining solution at room temperature for 10 min according to the manufacturer's instructions (Vazyme Biotech, Cat. A211).

The flow cytometry was processed by a flow cytometer (BD LSRFortessa™ Cell Analyzer, Cat. 647,800) with the FL1 channel for green fluorescence and the FL3 channel for red fluorescence.

HE staining

The zebrafish larvae in each group were fixed with 4% PFA at 4 ℃ for 12 h. Afterwards, each sample was dehydrated with gradient ethanol and paraffin-embedded. The dewaxed and hydrated 5 μm sections were stained with hematoxylin for 1 min and eosin for 30 s. The slides were mounted with neutral balsam and images were collected with a light microscope (Leica, DM2500) containing 40×/0.65 objectives.

RNA extraction and RNA-seq

The total RNA of zebrafish larvae at 120 hpf in each group ($N=15$) was isolated using RNAiso Plus (TakaRa, 9108) and stored at − 80 ℃. The concentration and purity of RNA were determined using a NanoPhotometer (ThermoFisher Scientific Intertek, Cat. 3,100,668).

RNA purification, cDNA synthesis, and RNA-Seq of each group ($N=3$) were performed by the Oebiotech company (Shanghai, China). RNA integrity was analyzed through the Agilent 2100 Bioanalyzer (Agilent Technologies, Santa Clara). The RNA integrity number ≥ 7 was subjected to the following analysis. The cDNA libraries were constructed using the TruSeq Stranded mRNA LTSample Prep Kit (Illumina, San Diego, CA, USA) and sequenced using the Illumina sequencing platform (HiSeq™ 2500). Raw data (raw reads) were conducted through Trimmomatic (Bolger et al. 2014). The reads, including ploy-N and low quality, were removed. Afterwards, the clean reads were mapped to the reference genome of *D. rerio* using hisat2 (Kim et al. 2015).

For differentially expressed genes (DEGs) analyses, the value of fragments per kilobase per million (FPKM) (Roberts et al. 2011) for each gene was calculated using cufflinks (Trapnell et al. 2010). The gene read counts were obtained through htseq-count (Anders et al. 2015). Then, each transcript was calculated using bowtie2 and eXpress (Roberts and Pachter 2013). DEGs were identified with DESeq R package functions estimate Size Factors and nbinom Test. $P<0.05$ and foldChange > 2 were set as the threshold for significantly differential expression.

KEGG (Kyoto Encyclopedia of Genes and Genomes) pathways and GO (Gene Ontology) analyses were conducted using the clusterProfiler R package based on the lists of DEGs for each treatment, respectively. The detailed procedure and data of RNA-Seq analysis were presented in supplemental materials and the NCBI Gene Expression Omnibus (Accession number: GSE193373).

Statistical analyses

All experiments in this study were duplicated three times. Statistical analyses were performed using GraphPad software (GraphPad Prism 8.0.1), Microsoft Excel (Microsoft Office 2013), and ImageJ software (ImageJ, 1.53c). The differences were analyzed via the two-way analysis of variance (two-way ANOVA) following Dunnett's test or the Student's *t*-test between control and different bepridil treatment groups. Data were shown as mean ± S.E.M. Ns, not significant. $*P<0.05$, $**P<0.01$, $***P<0.001$, and $****P<0.0001$.

Results

Effects of bepridil on cell proliferation of rat myocardial H9c2 cells

Presently, the cellular toxicity of bepridil in vitro cultured cells has not been reported. To explore the effects of bepridil on the viability and proliferation of myocardial cells, we used the stable rat myocardial cells H9c2 for short-term bepridil treatment.

We statistically analyzed that the viability IC_{50} of bepridil in H9c2 cells was 27 μM and $IC_{100} > 50$ μM (Supplementary Fig. 1a). Therefore, we mainly arranged two different bepridil groups (30 and 35 μM) in H9c2 cells and evaluated the drug responses. The trend of cell mortality in 30- and 35-μM bepridil treatment groups was consistent with the results of the CCK-8 assay. However, the surviving cells showed serious cytoplasmic vacuolization and nuclear abnormity in a concentration-dependent manner (Fig. 1a–e). These morphological changes might cause cell death.

Flow cytometry analysis showed an apparent apoptosis trend after 30-μM bepridil treatment. The cellular response to xenobiotic stimulus activated the cell apoptosis pathway (Fig. 1f-f'' and g-g''). In addition, the ROS signals in cells also increased significantly (Supplementary Fig. 1b-b''' and c). Many H9c2 cells stagnated in the G_1 phase or ceased to the G_0 phase after bepridil stimulation (Supplementary Fig. 1e-g). The cell cycle dynamics of the 30-μM bepridil treatment group also significantly reduced, and $81.73 \pm 1.58\%$ of the cells were in the G_0-G_1 phase (Supplementary Fig. 1e).

Assessment of bepridil embryotoxicity in D. rerio

To evaluate the effects of bepridil treatment during embryonic development, we specifically treated the zebrafish embryos with a serious concentration of bepridil from 24 to 120 hpf. We determined the LC_{10} (1295 ng/mL) of bepridil in zebrafish embryos (Fig. 2a). After 24 hpf, the zebrafish larva's circulatory system and internal organs underwent rapid morphogenesis. The early development of all zebrafish organs was completed at 120 hpf (Kimmel et al. 1995). We recorded the survival rate and the phenotype of each group at the hatching period, early larvae and late larvae periods, respectively (Fig. 2b–g'''').

As a result, we found that the mortality of embryos and larvae increased with the proportional drug doses and developmental stages (Fig. 2h, j). 3000 ng/mL of bepridil treatment resulted in a 100% mortality rate at 96 hpf. Meanwhile, bepridil treatment significantly affected the hatchability of zebrafish embryos (Fig. 2i). All individuals in 1250 ng/mL ($< LC_{10}$) bepridil-exposed group completed hatching until 120 hpf, and the hatching rate of the embryos was significantly decreased at 72 hpf ($83.33 \pm 3.85\%$) compared with the control group (100%). At 72 hpf, the hatching rate of embryos in 2000 ng/mL (LC_{50}) bepridil was $68.89 \pm 4.01\%$ and increased slightly to $74.44 \pm 6.19\%$ at 120 hpf. Taken together, bepridil treatment would affect and delay zebrafish embryo development.

It was worth mentioning that bepridil was more sensitive to zebrafish embryos than in vitro cultured rat myocardial cells H9c2, with an LC_{50} of 5.27 μM. We considered that early embryonic development was more complicated and more susceptible to environmental factors, especially drug intervention.

Effects of bepridil on the developmental morphology of zebrafish embryos

Except for delaying embryonic development, the zebrafish larvae showed different degrees of morphological abnormalities after bepridil treatment at 120 hpf, mainly including pericardium enlargement, yolk sac swelling, and tail bending. We divided the deformities into three degrees. The larvae with mild dysplasia manifested in abnormal pericardial pumping and a swollen pericardium (Fig. 3b', grade 1). The moderately defective larvae showed a more swollen pericardium. The yolk sac of the individual slightly bulged and bent the tail (Fig. 3b'', grade 2). In severely deformed larvae, the pericardium and abdominal cavity were greatly enlarged. Meanwhile, the blood circulation in the heart was hard to observe. The tail was short and curved seriously (Fig. 3 b''', grade 3). Individual larvae may also exhibit mild or severe deformities in low-concentration groups.

Statistical analysis revealed that the ratio of zebrafish larvae deformity was significantly aggravated with the increased dosage of bepridil (Fig. 3e). In the 1250-ng/mL ($< LC_{10}$) bepridil treatment group, the ratio of the deformity was $50.00 \pm 1.92\%$ at 120 hpf. We compared the body length of zebrafish larvae at 120 hpf (Fig. 3c), and the result was consistent with hatchability (Fig. 2i). The area of the yolk sac also increased, obviously after bepridil exposure (Fig. 3d). The number of severely deformed individuals increased with the drug concentration (Fig. 3e). Besides, the swim bladder was hard to distinguish after bepridil treatment (Fig. 3b'', b'''). Bepridil stimulation resulted in zebrafish embryonic growth retardation. Therefore, we confirmed that bepridil treatment could affect the development of zebrafish embryos and cause abnormal embryo morphology.

Besides, the transcriptome results showed several up-regulated apoptosis-related genes (caspase-3, caspase-6, caspase-7, caspase-8, caspase-9) and cell death-associated genes (*dap*, *dap1b*, *ing1*) in 120 hpf zebrafish larvae after bepridil exposure. Meanwhile, the connective tissue growth, cellular connection, and wnt pathway-associated factors resulted in negative regulation (Fig. 3f).

We also observed that the *bcl-2* related regulating/ interacting genes, *bnip3la* and *bnip3*, displayed up-regulation in 250 ng/mL group. Despite the embryos were alive and not show significant deformity, it suggested that low concentration of bepridil may also induced apoptosis during embryonic development. This result might explain the mild deformities in low concentration groups.

In addition, several cellular communication network factors (*ctgfb*, *wisp1b*, *wisp2,* and *wisp3*) showed an

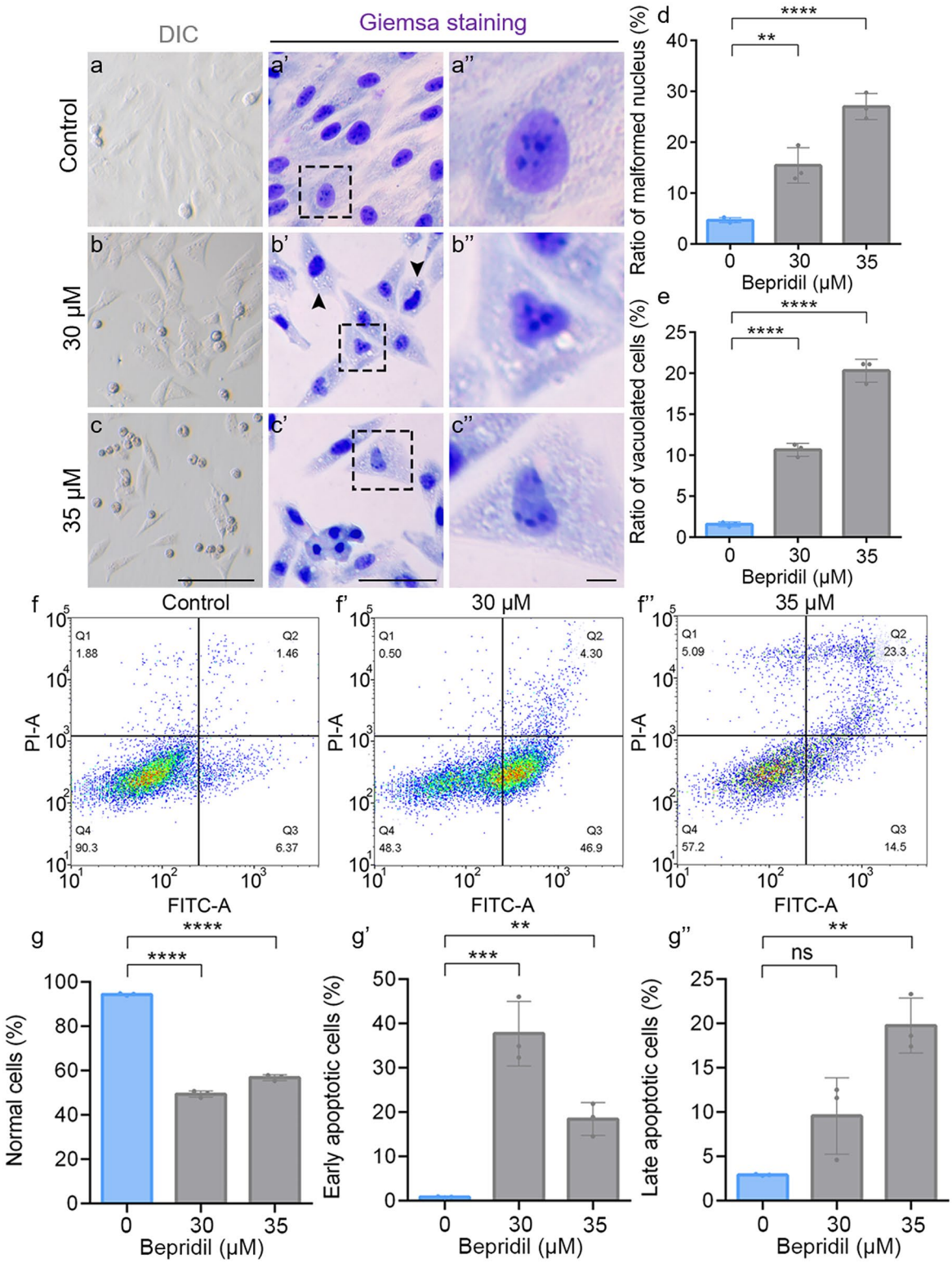

Fig. 1 Bepridil treatment results in cell apoptosis and morphological abnormality in H9c2 cells. (**a**-**c**'') Representative DIC and Giemsa staining phenotypes of H9c2 cells in Control, 30- and 35-μM bepridil treatment groups. Scale bars, 50 μm (general view) and 10 μm (zoom). (**d**, **e**) Quantification of the malformed nucleus and vacuolated cells in H9c2 after bepridil treatment in each group. (**f**-**f**'') Flow cytometry of Annexin V-FITC and PI co-staining cells in each group. (**g**-**g**'') The ratios of normal, early apoptotic and late apoptotic cells in different bepridil treated groups. The statistical significance was determined by the Student's *t*-test. $N=3$ for each group. Error bars, means ± SEM. ns, $P>0.05$; $^{**}P<0.01$, $^{***}P<0.001$, $^{****}P<0.0001$

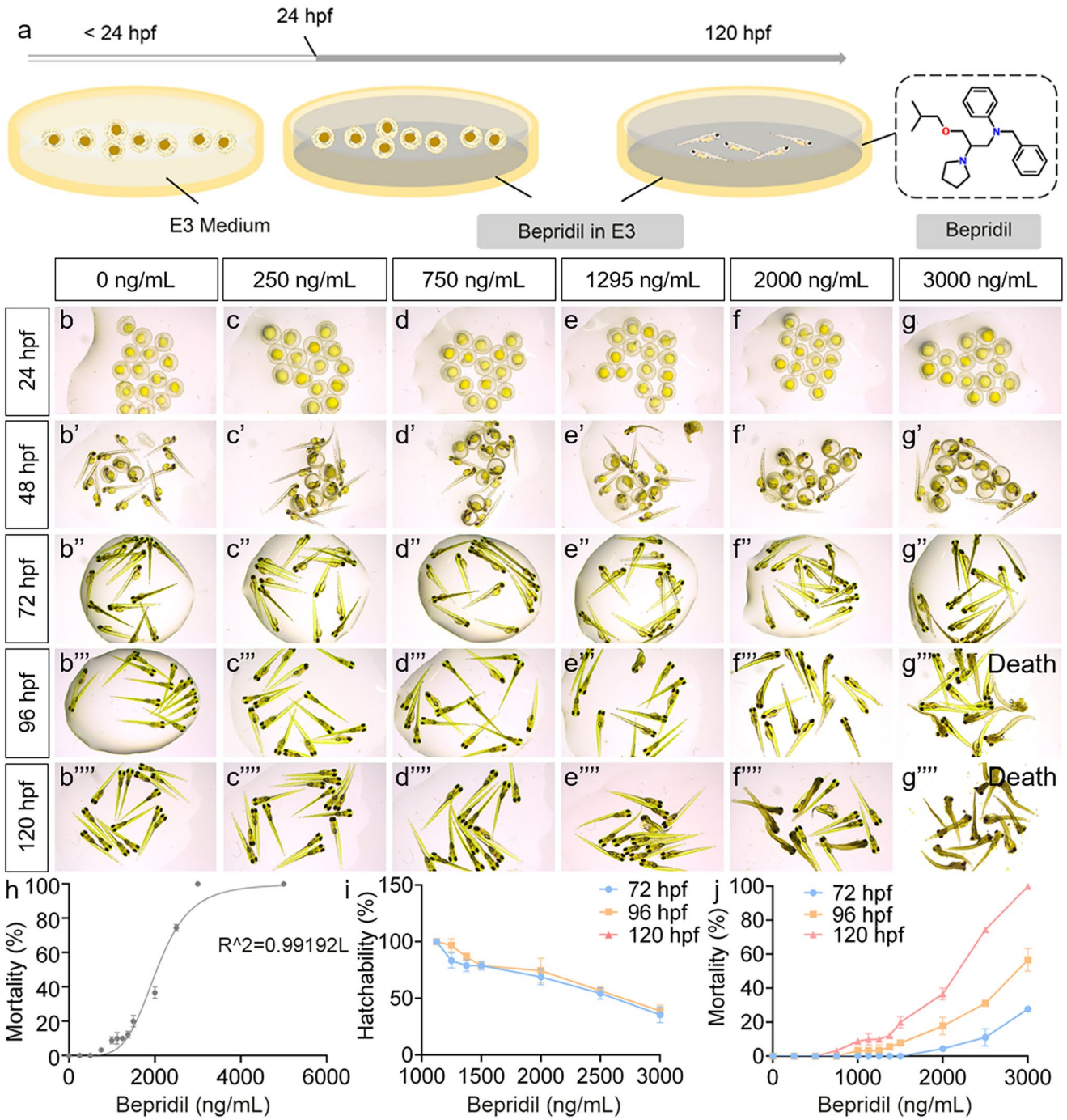

Fig. 2 Assessment of bepridil effects on zebrafish embryonic development. (**a**) Graphical model of in vivo bepridil treatment on zebrafish embryos. (**b**–**g**'''') The zebrafish embryos and larvae cultured in different concentrations of bepridil at 24, 48, 72, 96 and 120 hpf. 3000 ng/mL bepridil treatment resulted in 100% death at 96 and 120 hpf. $N=15$ per group. (**h**) The mortality of zebrafish exposed to different concentrations of bepridil. $LC_0=750.53$ ng/mL. $LC_{10}=1295.37$ ng/mL. $LC_{50}=2123.59$ ng/mL. $N=45$. (**i**) Correlationship and zebrafish hatchability of different bepridil concentrations at 72, 96, and 120 hpf. $N=45$. (**j**) Correlationship and zebrafish mortality of different bepridil concentrations at 72, 96 and 120 hpf. $N=45$

up-regulating tendency in low concentration of bepridil. Afterwards, these genes conversely down-regulated in the 1295 ng/mL group (Fig. 3f). The regulation of the wisp family members was considered functioning in postnatal skeletal growth, which implicated the potential effects of bepridil on embryonic bone development.

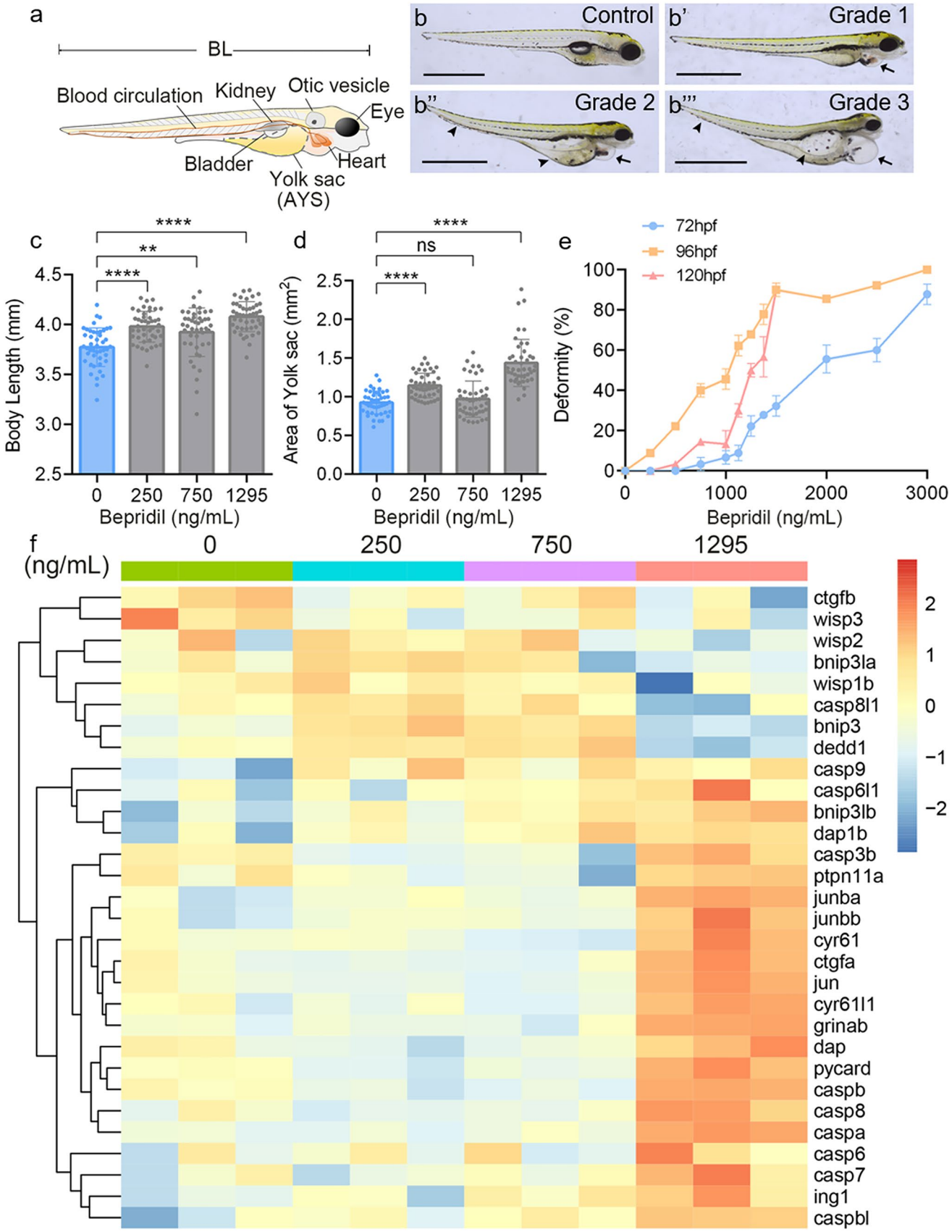
a
BL
Blood circulation
Kidney
Otic vesicle
Eye
Bladder
Heart
Yolk sac
(AYS)
b Control
b' Grade 1
b'' Grade 2
b''' Grade 3
c
Body Length (mm)
Bepridil (ng/mL)
d
Area of Yolk sac (mm2)
ns
Bepridil (ng/mL)
e
72hpf
96hpf
120hpf
Deformity (%)
Bepridil (ng/mL)
f
(ng/mL)
0
250
750
1295
ctgfb
wisp3
wisp2
bnip3la
wisp1b
casp8l1
bnip3
dedd1
casp9
casp6l1
bnip3lb
dap1b
casp3b
ptpn11a
junba
junbb
cyr61
ctgfa
jun
cyr61l1
grinab
dap
pycard
caspb
casp8
caspa
casp6
casp7
ing1
caspbl

◂**Fig. 3** Morphological effects of zebrafish larvae after bepridil treatment. (**a**) Diagram of zebrafish larva and the internal organs. BL, body length. AYS, area of the yolk sac. (**b**-**b**''') Bepridil treatment caused different degrees of deformity at 120 hpf. Grade 1, grade 2 and grade 3 represent the levels of deformity from low to high. Black arrows showed the pericardial enlargement. Black arrowheads indicated swollen yolk sacs and curved tails. Scale bars = 1 mm. (**c**) Body lengths of zebrafish larvae at 120 hpf in each group. $N = 45$. (**d**) Quantification of AYS in zebrafish larvae at 120 hpf in control and different bepridil groups. N = 45. (**e**) Correlationship and zebrafish deformity of different bepridil concentrations at 72, 96, and 120 hpf. $N = 45$. (**f**) Heatmap of cell apoptosis-related genes expression pattern in different bepridil treatment groups

Bepridil treatment resulted in cardiac developmental defects and myocardial weakness

After bepridil treatment, the AB line zebrafish showed obvious pericardial edema and blood circulation disorders. To confirm the effects of bepridil on embryonic cardiogenesis, transgenic *Tg (myl7:eGFP)* embryos were used for drug assessment in a parallel experiment. The vivid hearts of each zebrafish larva in different groups were recorded through time-lapse imaging (Videos 1–4). In the 1295-ng/mL bepridil treatment group, the zebrafish hearts were malformed with an abnormal cardiac rhythm. We captured the consecutive systolic and diastolic images and quantified the relative cardiac cycles (Supplementary Fig. 2a-d''''').

In addition, the bright-field videos of bepridil-exposed embryos showed that, in addition to hemodynamic changes of the systemic circulation, the heartbeats of zebrafish embryos decreased significantly (Videos 5–8; Supplementary Fig. 2e, f). We measured the distance between SV-BA and PA. The results showed the potential toxicity of bepridil on cardiac looping, and the PA would expand with the increase of bepridil concentration (Fig. 4a, d, e).

Through the confocal imaging of *my7:eGFP*, we found various abnormal heart looping during embryonic development, and the spatial positions of the atrium and ventricle were offset from the embryonic central axis (Fig. 4b-b'''). The cardiomyocytes of bepridil treatment groups showed similar histological features as the control group (Fig. 4c–c'''). Besides, the cardiac fluorescence area of zebrafish larvae at 120 hpf showed a significant decrease after 1295 ng/mL bepridil exposure (Fig. 4f). Despite the pericardial area showed no significant changes after low concentration of bepridil exposure (Fig. 4e; 250 ng/mL vs control, $P = 0.98$; 750 ng/mL vs control, $P = 0.88$), those individuals with normal phenotypes also presented dramatic heart rate reduction (Video 6, 7; Supplementary Fig. 2f). In addition, although the ratios of heart damage were approximately 80% in the 1295 ng/mL group, several zebrafish larvae retained normal phenotypes with obvious arrhythmia (Supplementary Fig. 2g; Video 8). We quantified the overall expression of my7:eGFP in individuals by confocal three-dimensional imaging. The results also confirmed that the pericardial edema response to bepridil treatment did not enlarge the structural chambers of the heart, on the contrary, it would reduce the volume of the heart (Fig. 4h, i'''). In brief, the morphological abnormalities of the heart during early embryonic development were directly proportional to the concentration of bepridil (Supplementary Fig. 2g).

In the transcriptome expression profile, we found several essential genes (*spns2*, *pdgfra*, and *npas4l*) that regulate myocardial predictor migration and endothelial cell proliferation had a dose-dependent down-regulation trend on bepridil treatment (Fig. 4g). The expression pattern of these factors was significantly decreased in 1295-ng/mL bepridil treatment group (Fig. 4g). Although the phenotype and organic development of zebrafish in low bepridil treatment groups (250 and 750 ng/mL) were similar to the wide type individuals, the heart morphogenesis-related transcription factors were downregulated. Especially, several crucial genes involved in mitochondrial respiration and TGF-β signaling.

Besides, the expression pattern of these genes showed the opposite result of upregulation in the 1295-ng/mL bepridil treatment group. The QT interval prolongation and bradycardia-related gene *atp1a1a.1* (Pott et al. 2018) showed a similar result (Fig. 4g). Thus, we suspected that bepridil treatment would lead to abnormal cardiovascular circulation and myocardial weakness. The disordered regulation of cardiac metabolism and cell proliferation may be a mechanism of organic compensatory responses.

Bepridil mainly affects the embryonic development of D. rerio by changing organic metabolism and myocardial contractility

To study the drug's metabolic mechanisms of pathophysiological changes, we compared the transcriptomes of zebrafish larvae after different concentrations of bepridil treatment. The principal component analysis (PCA) and clustering heatmap showed a consistent result, demonstrating the qualification of replication samples in each group.

The components of low concentration (250 and 750) and 1295-ng/mL bepridil treatment groups had great differences (Supplementary Fig. 3a, b). The overall gene expression profile revealed an up-regulated expression trend of most genes (Fig. 5c and Supplementary Fig. 4b). However, the result was opposite after 1295-ng/mL bepridil treatment (Fig. 5d). For volcanic clustering, most of the significantly changed factors ($P < 0.05$ and fold change > 2) showed negative expression in low concentrations of bepridil treatment (Fig. 5a and Supplementary Fig. 4a).

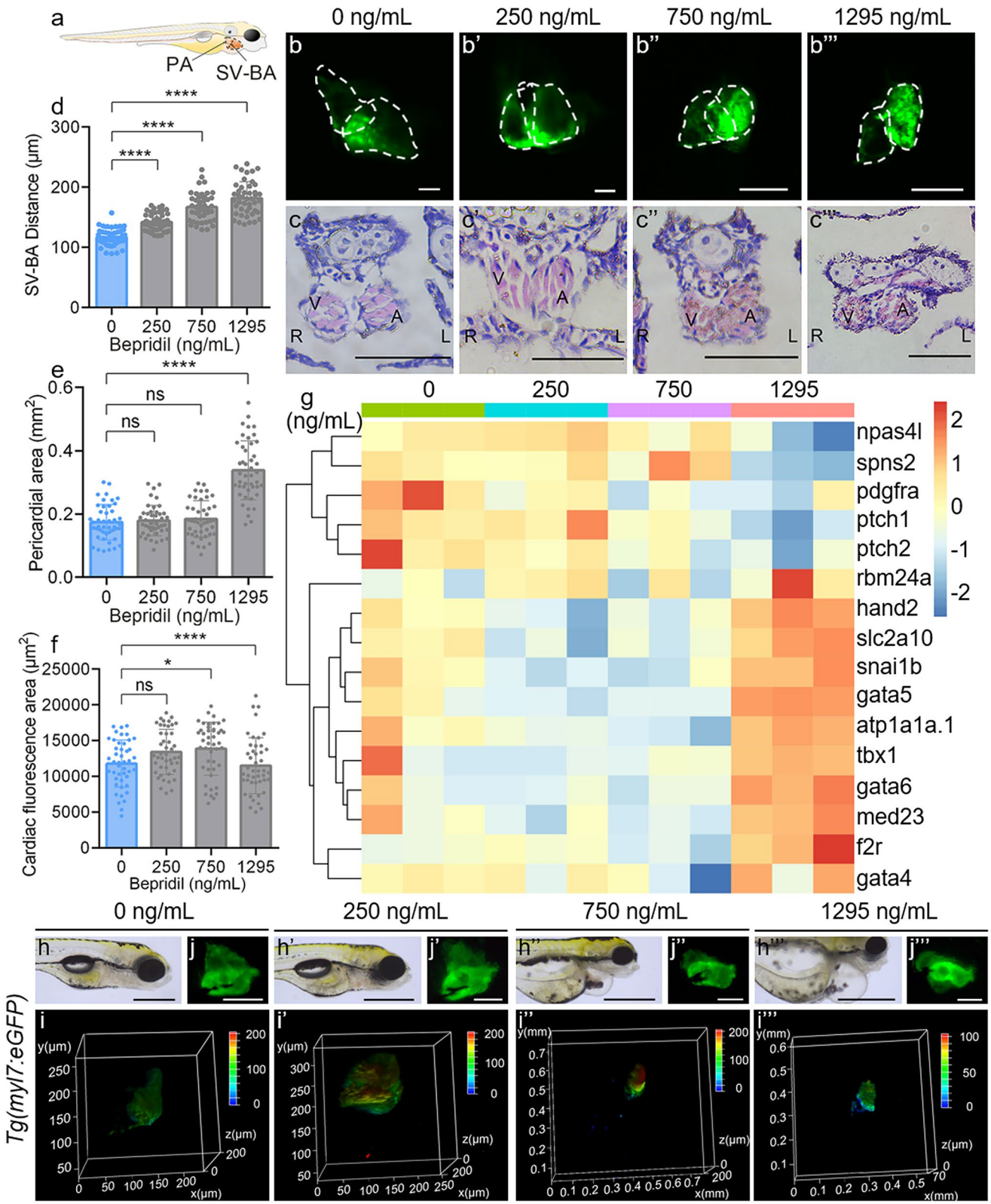

The RNA-seq data confirmed that low-dose of bepridil treatment induced an apparent xenobiotic stimulus and drug catabolic process. The enriched DEGs of GO and KEGG workflow showed negative regulation of proteolysis and peptidase in 250 and 750 ng/mL bepridil groups, which eventually led to the metabolic disorders of lipids and a

◂**Fig. 4** Bepridil-induced cardiac dysplasia on zebrafish embryonic development. (**a**) Graphical model for measuring the PA and distance of SV-BA in the larva. (**b**-**b**''') Representative confocal fluorescence and (**c**–**c**''') histological HE staining images of 120 hpf *Tg(myl7:eGFP)* zebrafish hearts in each group. Scale bars, 10 μm (fluorescence images) and 50 μm (HE staining). (**d**, **e**) SV-BA distance and PA were quantified at 120 hpf in the different doze of bepridil groups. $N=45$. ns, no significance. **P*-value < 0.05. *****P*-value < 0.0001. (**f**) Quantification of cardiac fluorescence areas at 120 hpf in control and treatment groups. (**g**) Cardiovascular development associated genes relative expression pattern at 120 hpf in different groups. (**h**–**h**''') Bright field, (**i**-**i**''') three-dimensional confocol fluorescence analyses and (**j**-**j**''') fluorescence representative images of *Tg(myl7:eGFP)* zebrafish hearts at 120 hpf in different groups. Scale bars = 100 μm (bright field) and 10 μm (fluorescence images)

variety of essential amino acids (Fig. 6a, c, Supplementary Fig. 5e, f and Supplementary Table S1).

As a long-term acting calcium antagonist, bepridil caused partial changes (Gene ratio, 61/426) of calcium signaling channel in 120 hpf zebrafish larvae after 1295 ng/mL (LC_{10}) treatment (NCBI Gene Expression Omnibus, No. GSE193373). However, the cardiac muscle contraction and adrenergic of cardiomyocytes were significantly affected in the same group (Fig. 6b, d). Besides, the overall DEGs were highly correlated to cell proliferation and regulation of cell transmembrane transports in the zebrafish (Fig. 6b). The RNA-seq results confirmed our hypothesis that bepridil treatment affected embryonic development, cardiogenesis, and cell viability.

Effects of bepridil on liver metabolism and hepatic functions

For KEGG enrichment, many DEGs were related to glucosamine, aminoglycan, sphingolipid, and amino acid metabolisms and steroid biosynthesis. One of the crucial organs responsible for these functions is the liver. Therefore, we speculated that the liver of zebrafish was also affected by bepridil during embryonic development.

We performed the bepridil treatment on the *Tg (fabp10a:dsRed)* zebrafish strain, specifically highlighting the hepatic cells in vivo. In the 1295-ng/mL bepridil treatment group, the general views of hepatic fluorescence signal were obviously decreased (Fig. 7a–e). A high-resolution confocal fluorescence microscope captured the most extensive fluorescence views (Fig. 7c–c'''). In three-dimensional imaging, the liver of zebrafish in the 1295-ng/mL bepridil treatment group also showed an ectopic and deficient spatial location (Fig. 7d-d'''). The down-regulated DEGs consisted of the hepatic branching and morphogenesis-associated genes (*zfyve9a* and *cdk5r1a*).

Meanwhile, the increased expression of *wnt* and *snapc2* manifested in abnormal hepatic cellular polar migration. In the ROS and apoptosis assay results, bepridil treatment showed an increasing accumulation of ROS and apoptotic cells, mainly in the caudal hematopoietic tissue (Supplementary Fig. 5a-d'').

We compared the individual histological characteristics between control and bepridil treatment groups according to the potential toxicity of bepridil on neurodevelopment. The nerve and brain stromal cells in dorsal and ventral telencephalon areas lacked cell connections and disordered the brain sub-regions (Supplementary Fig. 6a-d''). The optic cells dispersed in the inner and outer nuclear layers, and the inner plexiform layer showed abnormal pigment deposition (Supplementary Fig. 6a-d'').

Discussion

Rat H9c2 myocardial cells are commonly used to verify the cardiotoxicity of drugs. Cytoplasmic vacuolization responds to foreign bioactive chemicals, which result in intracellular organic amine accumulation and low pH. Afterwards, the lysosome, endosome, autolysosome, or endoplasmic reticulum expanded as well as homotypic fused together (Aki et al. 2012). In contrast, microcytosis produces vacuolar expansion with non-cellular organelles. In this way, the vacuoles can be reversed, typically in metabolism (Gao et al. 2021). Gao et al. (2021) assessed the toxicity of maduramicin, a traditional animal coccidiostat, using H9c2 cells and observed the reversible vacuolization. It was transparent and consisted of a single membrane.

As demonstrated in our results, bepridil treatment resulted in the formation of dense and smaller vacuoles in H9c2 cells. This vacuole could not be reversed and resulted in changes to the nuclear morphology and cell death (Fig. 1a–c''). The result was analogous to the abnormality associated with endocytosis of the lysosome pathway. Therefore, we hypothesized that bepridil entered cells primarily via endocytosis.

The complex pharmacology of bepridil is manifested in multi-ion transmembrane inhibition. The transcriptomes of our zebrafish model showed that bepridil was involved in metal ion transports and regulated inorganic cation transport and chemical synaptic transmission (Fig. 6). The abnormal regulation of cell transmembrane may lead to the accumulation of organic amines in cells via organic cation delivery (Koepsell et al. 2007). Although bepridil showed an inhibitory effect in the apoptotic HL-1 cell model (Endo et al. 2013), in our results, both H9c2 cells and zebrafish larvae reflected a significant increase in ROS and activated cell apoptosis. This opposite effect may be associated with different cell types and medication methods.

In the zebrafish model, the embryos initiated taking bepridil at 24 hpf, and the drug treatment went through the whole process of early embryonic development. During the

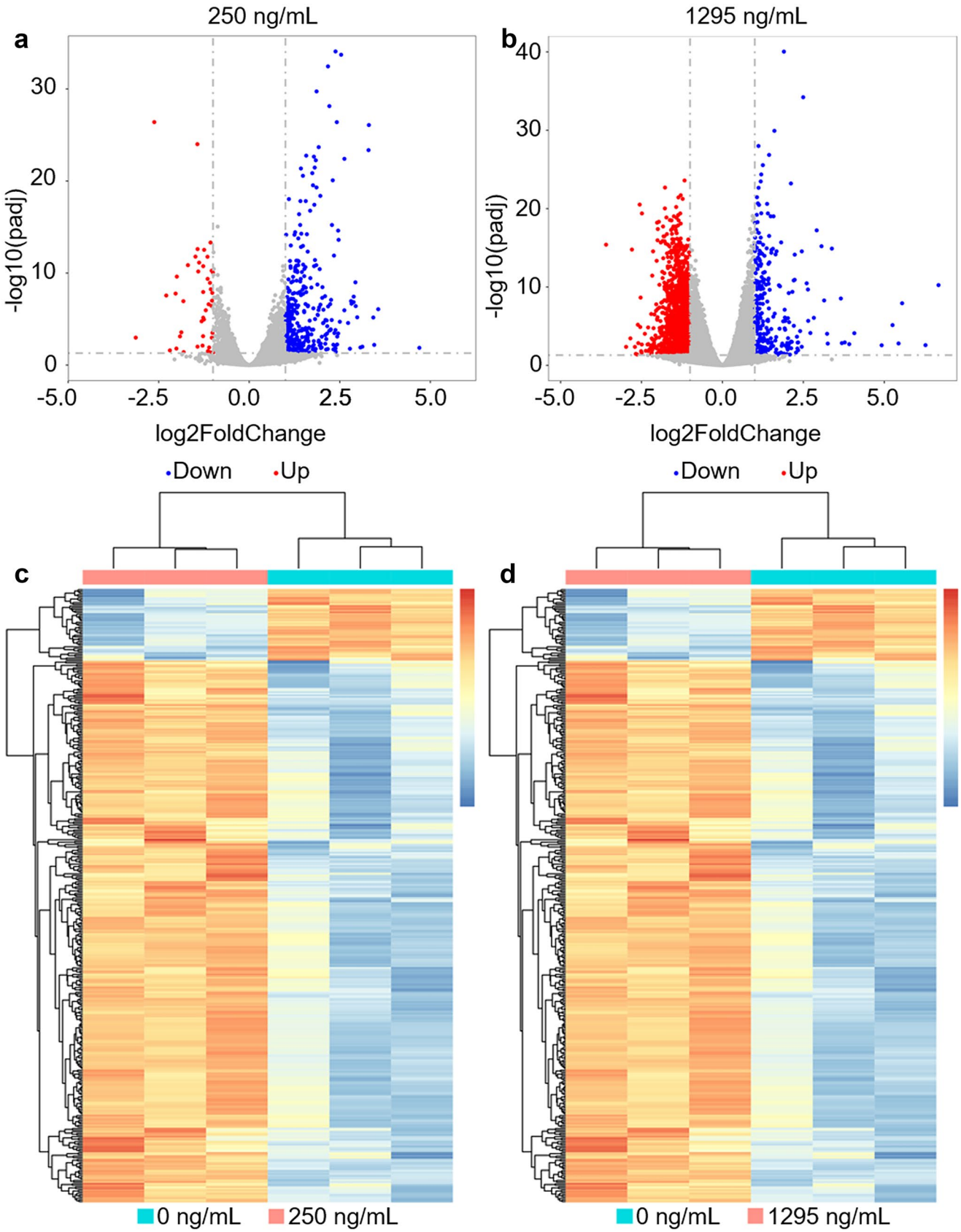
a
250 ng/mL
-log10(padj)
log2FoldChange
Down
Up
b
1295 ng/mL
-log10(padj)
log2FoldChange
Down
Up
c
0 ng/mL
250 ng/mL
d
0 ng/mL
1295 ng/mL

◂**Fig. 5** Different doses of bepridil treatment caused the alteration of most gene expression profiles in zebrafish organisms. **a**, **b** The volcano plot significantly changed genes in 250- and 1295-ng/mL bepridil treatment groups compared with control (*P*-values < 0.05, fold change > 2). Blue and red plots show down-regulated and up-regulated changed genes, respectively. **c**, **d** Hierarchical clustering heatmaps display the differential gene expression pattern between control and bepridil treatment groups (250 and 1295 ng/mL). The differential genes were normalized by FPKM expression values (adjusted *P*-values < 0.05, fold change > 2). For colorimetric scale, red and blue represent up-regulated and down-regulated genes

pharyngula period (24–48 hpf), the body axis around the yolk sac gradually straightens with the development of the circulatory system, pigment, and fins (Kimmel et al. 1995).

For cardiac development, bilateral cardiac precursor cells and endothelial cell layer fuse at the midline and form a cardiac disc at 22 hpf (25-somite) (Bakkers 2011). Then, the cardiomyocytes migrate and loop to generate the cardiac tube. The epicardium develops to cover the myocardium with cardiogenic differentiation and completes the early morphological development of the zebrafish heart at 48 hpf (Alfano et al. 2019; Bakkers 2011; Chen et al. 2020; Qiao et al. 2014; Wen et al. 2017). According to our findings, bepridil enlarged the chambers of the atrium and ventricle while decreasing their spatial positions. The zebrafish larva's pericardium was swollen and protruding, and the cardiac apex could not be distinguished (Figs. 3, 4).

The RNA-seq data of this study enriched several essential factors that mainly involve myocardial progenitor cell migration. During cardiac disc formation, both *spns2* and *pdgfra* regulate the movement of the endocardium and myocardial cell layer to the lateral mesoderm (El-Rass et al. 2017; Kawahara et al. 2009). While they resulted in significant decreases in gene expression following bepridil treatment (Fig. 4g), Bepridil was found to decrease cardiac contractility in adults (Zeller and Spinler 1987). However, it also affected mitochondrial respiration and TGF signaling during the development of the cardiovascular system (Poon et al. 2012; Willaert et al. 2012). As a result of the deformed embryonic heart, cardiac self-repair and fibrosis de fibrosis may be induced (Fig. 4g).

The up-regulation of several heart-specific genes in high-dose bepridil-treated embryos implied our hypothesis (Fig. 4g). These genes are essential for myocardial differentiation, cardiac primordia migration, as well as cardiac valve and second heart field morphogenesis (Ellertsdottir et al. 2012; Gentile et al. 2021; Nevis et al. 2013; Sam et al. 2020; Schindler et al. 2014). Especially the zinc finger transcription factors (*gata4/5/6*). Cardiac specification depends on the overall dosage and certain pairs of *gata4/5/6* genes (Sam et al. 2020). Overexpression of *gata5* resulted in the ectopic foci of beating myocardial tissue and altered the expression of many other myocardial genes (Reiter et al. 1999). During embryonic cardiogenesis, overexpression of hand2 induced an enlarged heart and the outflow tract (Schindler et al. 2014). Likewise, *hand2* is highly related to the patterning of the anterior lateral plate mesoderm.

The hemodynamic changes are associated with the development of vascular smooth muscle and cardiovascular disorders. For instance, *Npas4l* determined the development of vascular smooth muscle cells (Marass et al. 2019), and its expression pattern decreased obviously in the 1295-ng/mL bepridil treatment group. Bepridil increases Ca^{2+} current in mitochondria by regulating and inhibiting Na^{+} exchange, thereby decreasing cardiomyocyte contraction (Tari et al. 1987). Cellular energy is dependent on mitochondrial ATP production, which is dependent on intracellular calcium (Duchen et al. 2008). Bepridil treatment on a long-term basis has an effect on the balances of Na^{+}, K^{+}, and Ca^{2+} movements (Kang et al. 2009). We hypothesized that the accumulation of calcium in the mitochondria could result in cardiac dysfunction and neural cell death, particularly during embryonic development. That is why zebrafish larvae demonstrate pathological changes in their heart and brain tissues.

During the hatching periods of *D. rerio* (48–72 hpf), all primitive organs initiate morphogenesis (Kimmel et al. 1995). In this process, the hepatic cells proliferate rapidly due to the growth factors. *Cdk5r1a*, *snapc2*, and *zfyve9a* act as regulators of hepatic epithelial cells, resulting in the formation of an intrahepatic biliary network (Dimri et al. 2017; Liu et al. 2013; Schaub et al. 2012). The disordered cell proliferation and differentiation of hepatic precursor cells resulted in a spatial compression of pancreatic and anterior intestinal tissues (Poulain and Ober 2011). In our transcripts, *wnt2* showed a significant upregulation after bepridil treatment, suggesting the liver had a positive ectopic localization (Poulain and Ober 2011). This explains why we could not observe regular and complete liver in the 1295-ng/mL bepridil treatment group (Fig. 7a'''–d''').

Generally, bepridil treatment induces embryotoxicity during zebrafish development, which results in growth postponement and abnormal organic morphogenesis. Body length and phenotypic defects are exacerbated in a concentration-dependent manner by bepridil. Although a low dose of bepridil had no effect on myocardial contraction or ion transport channels, the transcriptomes of many genes involved in the early cardiovascular formation and liver maturation were significantly downregulated (Figs. 4g and 7f). Additionally, we cannot estimate the toxic effects of bepridil on lung stroma and lung formation using our zebrafish model. Bepridil has been extensively studied as a traditional Ca^{2+} channel inhibitor in a variety of research fields, let alone its use in anti-arrhythmia in several countries. It is critical to further elucidate the pharmacodynamic effects and toxicological mechanisms of bepridil.

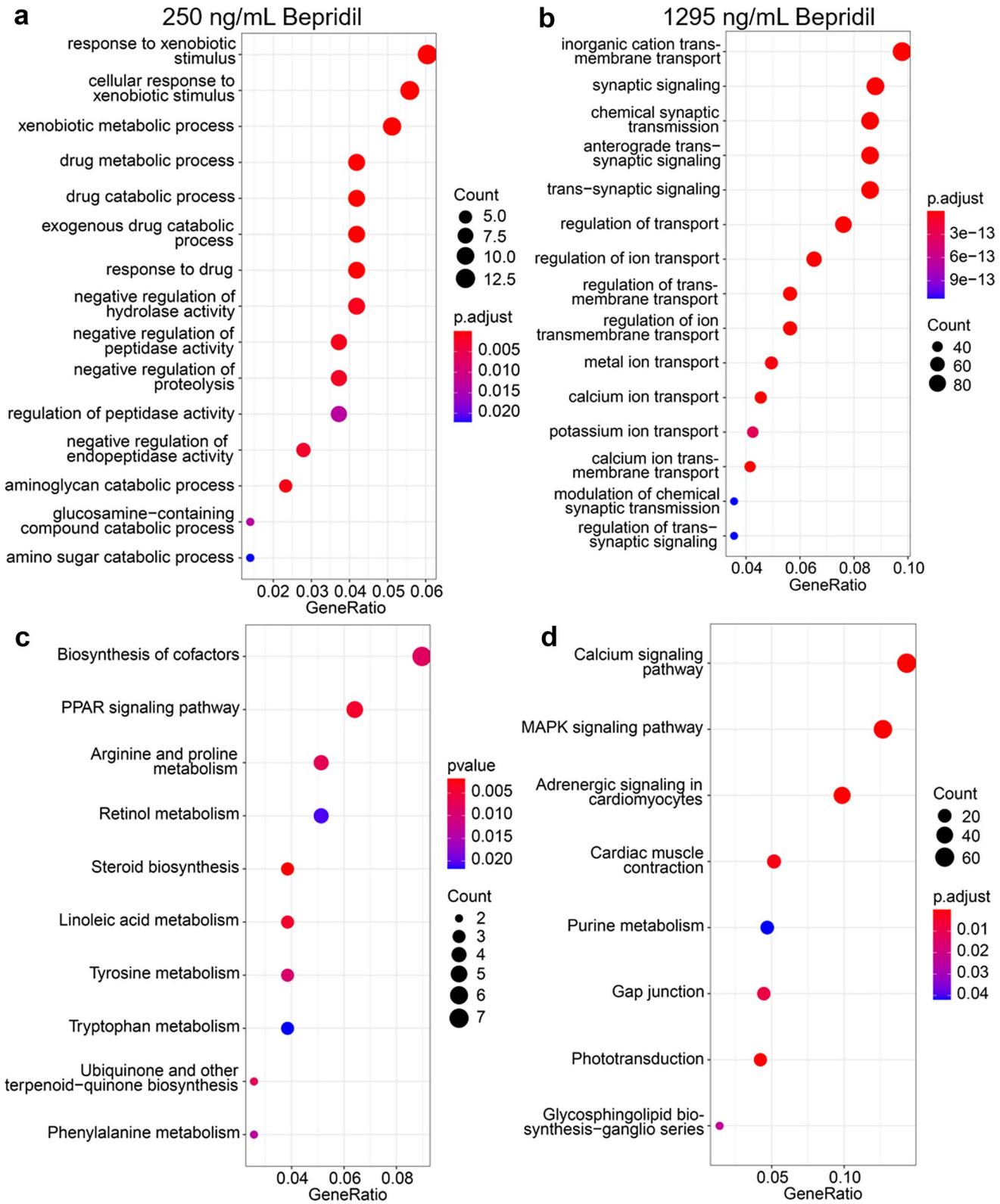

Fig. 6 Different doses of bepridil treatment resulted in differential drug responses, metabolism and biosynthesis in zebrafish. **a**, **b** GO and KEGG enrichment analysis between the control and 250 ng/mL bepridil treatment group. **c**, **d** GO and KEGG enrichment analysis between the control and 1295 ng/mL bepridil treatment group

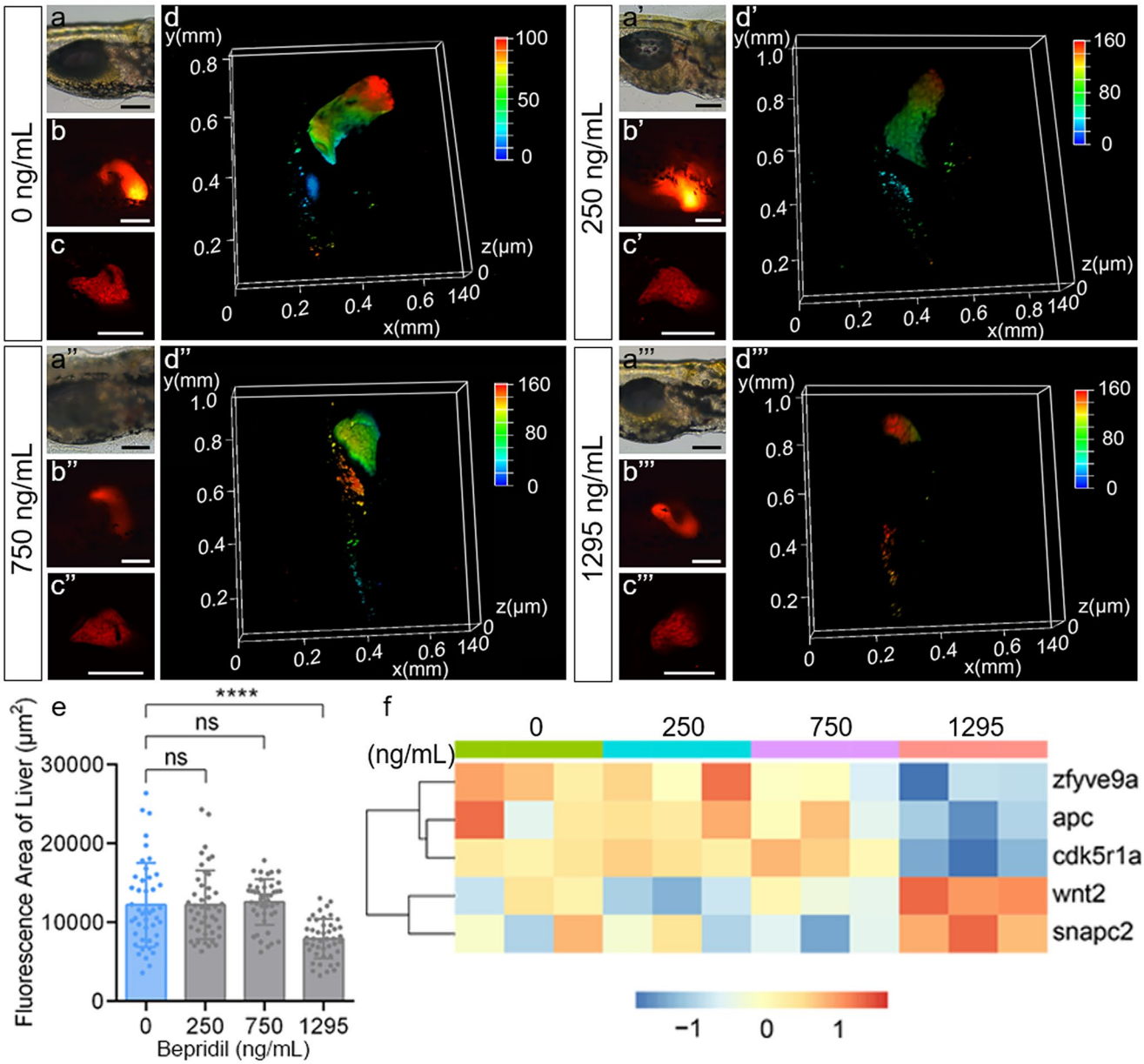

Fig. 7 Bepridil treatment caused hepatic defects during the embryonic development of zebrafish. (**a**-**a**''') Representative bright field, (**b**-**b**''') regular fluorescence images, (**c**–**c**''') confocol fluorescence images, and (**d**-**d**''') three-dimensional confocol fluorescence analyses of *Tg(fabp10a:dsRed)* zebrafish livers at 120 hpf in control and different dozes of bepridil treatment groups. Scale bar = 200 μm. (**e**) Quantification of hepatic fluorescence areas at 120 hpf in control and different dozes of bepridil groups. Error bars, mean ± S.E.M. $N = 45$. (**f**) Heatmap of mRNA expression pattern of hepatic development associated genes in 0, 250, 750, and 1295 ng/mL bepridil treatment groups at 120 hpf

Supplementary Information The online version contains supplementary material available at https://doi.org/10.1007/s00441-022-03706-w.

Author contribution Ya-Lan Wei: conceptualization, methodology, data curation, writing—original draft, and writing—review and editing. Yu-Qing Lei: methodology, data curation, and writing—original draft. Zhou-Jie Ye: project administration and resources. Xu-Dong Zhuang: data curation, validation, and software. Li-Ping Zhu: data curation and visualization. Xin-Rui Wang: conceptualization, methodology, project administration, and supervision. Hua Cao: conceptualization, supervision, and funding acquisition.

Funding This study was supported by the grants from the Natural Science Foundation of Fujian Province, China (No. 2020J01344), the Key Project on the Integration of Industry, Education and Research Collaborative Innovation of Fujian Province (No. 2021YZ034011), the Key Project on Science and Technology Program of Fujian Health Commission (No. 2021ZD01002).

Declarations

Ethical approval All zebrafish experiments were performed following the guidance and administration of the Animal Research Committee at Fujian Maternity and Child Health Hospital (License No. 2021KLRD649).

Informed consent Not applicable.

Conflict of interest The authors declare that they have no conflict of interest.

References

Alfano D, Altomonte A, Cortes C, Bilio M, Kelly RG, Baldini A (2019) Tbx1 regulates extracellular matrix-cell interactions in the second heart field. Hum Mol Genet 28:2295–2308. https://doi.org/10.1093/hmg/ddz058

Aizawa Y, Yamakawa H, Takatsuki S, Katsumata Y, Nishiyama T, Kimura T et al (2013) Efficacy and safety of bepridil for prevention of ICD shocks in patients with Brugada syndrome and idiopathic ventricular fibrillation. Int J Cardiol 168:5083–5085. https://doi.org/10.1016/j.ijcard.2013.07.187

Aki T, Nara A, Uemura K (2012) Cytoplasmic vacuolization during exposure to drugs and other substances. Cell Biol Toxicol 28:125–131. https://doi.org/10.1007/s10565-012-9212-3

Anders S, Pyl PT, Huber W (2015) HTSeq–a Python framework to work with high-throughput sequencing data. Bioinformatics 31:166–169. https://doi.org/10.1093/bioinformatics/btu638

Bakkers J (2011) Zebrafish as a model to study cardiac development and human cardiac disease. Cardiovasc Res 91:279–288. https://doi.org/10.1093/cvr/cvr098

Baldoni S, Del Papa B, Dorillo E, Aureli P, De Falco F, Rompietti C et al (2018) Bepridil exhibits anti-leukemic activity associated with NOTCH1 pathway inhibition in chronic lymphocytic leukemia. Int J Cancer 143:958–970. https://doi.org/10.1002/ijc.31355

Bolger AM, Lohse M, Usadel B (2014) Trimmomatic: a flexible trimmer for Illumina sequence data. Bioinformatics 30:2114–2120. https://doi.org/10.1093/bioinformatics/btu170

Carlisle MA, Fudim M, DeVore AD, Piccini JP (2019) Heart failure and atrial fibrillation, like fire and fury. JACC Heart Fail 7:447–456. https://doi.org/10.1016/j.jchf.2019.03.005

Chen H, Sun W, Zhu J, Yuan H, Chu M, Wen B (2020) Modification of cardiac transcription factor Gata6 by SUMO. Biochimie 170:212–218. https://doi.org/10.1016/j.biochi.2020.01.014

DeWald LE, Dyall J, Sword JM, Torzewski L, Zhou H, Postnikova E et al (2018) The calcium channel blocker bepridil demonstrates efficacy in the murine model of marburg virus disease. J Infect Dis 218:S588–S591. https://doi.org/10.1093/infdis/jiy332

Duchen MR, Verkhratsky A, Muallem S (2008) Mitochondria and calcium in health and disease. Cell Calcium 44:1–5. https://doi.org/10.1016/j.ceca.2008.02.001

Dimri M, Bilogan C, Pierce LX, Naegele G, Vasanji A, Gibson I et al (2017) Three-dimensional structural analysis reveals a Cdk5-mediated kinase cascade regulating hepatic biliary network branching in zebrafish. Development 144:2595–2605. https://doi.org/10.1242/dev.147397

El-Rass S, Eisa-Beygi S, Khong E, Brand-Arzamendi K, Mauro A, Zhang H et al (2017) Disruption of pdgfra alters endocardial and myocardial fusion during zebrafish cardiac assembly. Biol Open 6:348–357. https://doi.org/10.1242/bio.021212

Ellertsdottir E, Berthold PR, Bouzaffour M, Dufourcq P, Trayer V, Gauron C et al (2012) Developmental role of zebrafish protease-activated receptor 1 (PAR1) in the cardio-vascular system. PLoS ONE 7:e42131. https://doi.org/10.1371/journal.pone.0042131

Endo R, Notsu T, Mishima M, Morikawa K, Li P, Ikeda N et al (2013) Bepridil suppresses apoptosis in HL-1 cardiac atrial myocytes expressing mutant E334K cMyBPC. Yonago Acta Med 56:93–95

Gaku S, Naoshi K, Teruhiko A (2003) A case of bepridil induced interstitial pneumonitis. Heart 89:1415. https://doi.org/10.1136/heart.89.12.1415

Gao X, Ji C, Wang J, Song X, Zuo R, Zhang J et al (2021) Maduramicin induces cardiotoxicity via Rac1 signaling-independent methuosis in H9c2 cells. J Appl Toxicol 41:1937–1951. https://doi.org/10.1002/jat.4175

Garcia ML, Slaughter RS, King VF, Kaczorowski GJ (1988) Inhibition of sodium-calcium exchange in cardiac sarcolemmal membrane vesicles. 2. Mechanism of Inhibition by Bepridil Biochemistry 27:2410–2415. https://doi.org/10.1021/bi00407a024

Gentile A, Bensimon-Brito A, Priya R, Maischein HM, Piesker J, Guenther S et al (2021) The EMT transcription factor Snai1 maintains myocardial wall integrity by repressing intermediate filament gene expression. Elife 10:e66143. https://doi.org/10.7554/eLife.66143

Hasegawa GR (1988) Nicardipine, nitrendipine, and bepridil: new calcium antagonists for cardiovascular disorders. Clin Pharm 7:97–108

Hill JA, O'Brien JT, Alpert JS, Gore JM, Zusman RM, Christensen D et al (1985) Effect of bepridil in patients with chronic stable angina: results of a multicenter trial. Circulation 71:98–103. https://doi.org/10.1161/01.cir.71.1.98

Hollingshead LM, Faulds D, Fitton A (1992) Bepridil. A review of its pharmacological properties and therapeutic use in stable angina pectoris. Drugs 44:835–857. https://doi.org/10.2165/00003495-199244050-00009

Kang L, Zheng MQ, Morishima M, Wang Y, Kaku T, Ono K (2009) Bepridil up-regulates cardiac Na^+ channels as a long-term effect by blunting proteasome signals through inhibition of calmodulin activity. Br J Pharmacol 157:404–414. https://doi.org/10.1111/j.1476-5381.2009.00174.x

Kawamura M, Munetsugu Y, Tanno K, Kobayashi Y (2013) Carvedilol is effective and safe in combination with bepridil for persistent atrial fibrillation and decreases the QT prolongation induced by bepridil therapy. J Cardiovasc Pharmacol 61:77–82. https://doi.org/10.1097/FJC.0b013e3182790692

Kawahara A, Nishi T, Hisano Y, Fukui H, Yamaguchi A, Mochizuki N (2009) The sphingolipid transporter spns2 functions in migration of zebrafish myocardial precursors. Science 323:524–527. https://doi.org/10.1126/science.1167449

Kim D, Langmead B, Salzberg SL (2015) HISAT: a fast spliced aligner with low memory requirements. Nat Methods 12:357–360. https://doi.org/10.1038/nmeth.3317

Kimmel CB, Ballard WW, Kimmel SR, Ullmann B, Schilling TF (1995) Stages of embryonic development of the zebrafish. Dev Dyn 203:253–310. https://doi.org/10.1002/aja.1002030302

Koepsell H, Lips K, Volk C (2007) Polyspecific organic cation transporters: structure, function, physiological roles, and biopharmaceutical implications. Pharm Res 24:1227–1251. https://doi.org/10.1007/s11095-007-9254-z

Liu N, Li Z, Pei D, Shu X (2013) Zfyve9a regulates the proliferation of hepatic cells during zebrafish embryogenesis. Int J Dev Biol 57:773–778. https://doi.org/10.1387/ijdb.130065xs

Marass M, Beisaw A, Gerri C, Luzzani F, Fukuda N, Günther S et al (2019) Genome-wide strategies reveal target genes of Npas4l associated with vascular development in zebrafish. Development 146:dev173427. https://doi.org/10.1242/dev.173427

Milan DJ, Peterson TA, Ruskin JN, Peterson RT, MacRae CA (2003) Drugs that induce repolarization abnormalities cause bradycardia in zebrafish. Circulation 107:1355–1358. https://doi.org/10.1161/01.cir.0000061912.88753.87

Mitterreiter S, Page RM, Kamp F, Hopson J, Winkler E, Ha HR et al (2010) Bepridil and amiodarone simultaneously target the Alzheimer's disease beta- and gamma-secretase via distinct mechanisms. J Neurosci 30:8974–8983. https://doi.org/10.1523/JNEUROSCI.1199-10.2010

Nevis K, Obregon P, Walsh C, Guner-Ataman B, Burns CG, Burns CE (2013) Tbx1 is required for second heart field proliferation in zebrafish. Dev Dyn 242:550–559. https://doi.org/10.1002/dvdy.23928

Nishino M, Mori N, Nakamura D, Lee Y, Yoshimura T, Taniike M et al (2013) Correlation between inflammation state and successful medical cardioversion using bepridil for refractory atrial fibrillation. J Cardiol 62:117–120. https://doi.org/10.1016/j.jjcc.2013.03.003

Pettit SD, Berridge B, Sarazan RD (2010) A call for more integrated cardiovascular safety assessment. J Pharmacol Toxicol Methods 61:1–2. https://doi.org/10.1016/j.vascn.2009.08.001

Poon KL, Tan KT, Wei YY, Ng CP, Colman A, Korzh V et al (2012) RNA-binding protein RBM24 is required for sarcomere assembly and heart contractility. Cardiovasc Res 94:418–427. https://doi.org/10.1093/cvr/cvs095

Poulain M, Ober EA (2011) Interplay between Wnt2 and Wnt2bb controls multiple steps of early foregut-derived organ development. Development 138:3557–3568. https://doi.org/10.1242/dev.055921

Pott A, Bock S, Berger IM, Frese K, Dahme T, Keßler M et al (2018) Mutation of the Na^+/K^+-ATPase Atp1a1a.1 causes QT interval prolongation and bradycardia in zebrafish. J Mol Cell Cardiol 120:42–52. https://doi.org/10.1016/j.yjmcc.2018.05.005

Qiao L, Gao H, Zhang T, Jing L, Xiao C, Xiao Y et al (2014) Snail modulates the assembly of fibronectin via α5 integrin for myocardial migration in zebrafish embryos. Sci Rep 4:4470. https://doi.org/10.1038/srep04470

Ramlakhan KP, Johnson MR, Roos-Hesselink JW (2020) Pregnancy and cardiovascular disease. Nat Rev Cardiol 17:718–731. https://doi.org/10.1038/s41569-020-0390-z

Reiter JF, Alexander J, Rodaway A, Yelon D, Patient R, Holder N et al (1999) Gata5 is required for the development of the heart and endoderm in zebrafish. Genes Dev 13:2983–2995. https://doi.org/10.1101/gad.13.22.2983

Ren J, Zhao Y, Fry EE, Stuart DI (2018) Target identification and mode of action of four chemically divergent drugs against ebolavirus infection. J Med Chem 61:724–733. https://doi.org/10.1021/acs.jmedchem.7b01249

Roberts A, Pachter L (2013) Streaming fragment assignment for real-time analysis of sequencing experiments. Nat Methods 10:71–73. https://doi.org/10.1038/nmeth.2251

Roberts A, Trapnell C, Donaghey J, Rinn JL, Pachter L (2011) Improving RNA-Seq expression estimates by correcting for fragment bias. Genome Biol 12:R22. https://doi.org/10.1186/gb-2011-12-3-r22

Sam J, Mercer EJ, Torregroza I, Banks KM, Evans T (2020) Specificity, redundancy and dosage thresholds among gata4/5/6 genes during zebrafish cardiogenesis. Biol Open 9:bio053611. https://doi.org/10.1242/bio.053611

Sato N, Nishimura M, Kawamura Y, Ward CA, Kikuchi K (1996) Block of Na^+ channel by bepridil in isolated guinea-pig ventricular myocytes. Eur J Pharmacol 314:373–379. https://doi.org/10.1016/s0014-2999(96)00567-5

Schaub M, Nussbaum J, Verkade H, Ober EA, Stainier DY, Sakaguchi TF (2012) Mutation of zebrafish Snapc4 is associated with loss of the intrahepatic biliary network. Dev Biol 363:128–137. https://doi.org/10.1016/j.ydbio.2011.12.025

Schindler YL, Garske KM, Wang J, Firulli BA, Firulli AB, Poss KD et al (2014) Hand2 elevates cardiomyocyte production during zebrafish heart development and regeneration. Development 141:3112–3122. https://doi.org/10.1242/dev.106336

Suzuki T, Hanaoka M, Yokoyama T, Koizumi T, Kubo K (2009) Gradual progression of interstitial pneumonia induced by bepridil. Intern Med 48:2033–2035. https://doi.org/10.2169/internalmedicine.48.2490

Tari C, Fournier N, Ducet G, Crevat A, Albengres E, Urien S et al (1987) Comparative study of bepridil and nicardipine action on respiration and calcium transport in mitochondria. Int J Clin Pharmacol Ther Toxicol 25:26–30

Trapnell C, Williams BA, Pertea G, Mortazavi A, Kwan G, van Baren MJ et al (2010) Transcript assembly and quantification by RNA-Seq reveals unannotated transcripts and isoform switching during cell differentiation. Nat Biotechnol 28:511–515. https://doi.org/10.1038/nbt.1621

Tsubota M, Matsui K, Fukushi S, Okazaki K, Sekiguchi F, Kawabata A (2021) Effects of bepridil and pimozide, existing medicines capable of blocking T-type Ca^{2+} channels, on visceral pain in mice. Biol Pharm Bull 44:461–464. https://doi.org/10.1248/bpb.b20-00742

van Veenendaal NR, Ulmer B, Boskovski MT, Fang X, Khokha MK, Wendler CC et al (2013) Embryonic exposure to propylthiouracil disrupts left-right patterning in Xenopus embryos. FASEB J 27:684–691. https://doi.org/10.1096/fj.12-218073

Vatansever EC, Yang KS, Drelich AK, Kratch KC, Cho CC, Kempaiah KR et al (2021) Bepridil is potent against SARS-CoV-2 in vitro. Proc Natl Acad Sci U S A 118:e2012201118. https://doi.org/10.1073/pnas.2012201118

Wang Y, Fu Z, Ma Z, Li N, Shang H (2021) Bepridil, a class IV antiarrhythmic agent, can block the TREK-1 potassium channel. Ann Transl Med 9:1123. https://doi.org/10.21037/atm-20-7971

Watanabe M, Takata Y, Fukasawa S, Sakota K, Abe T, Goseki Y et al (2009) Two patients with bepridil-induced interstitial pneumonia. Circ J 73:1352–1355. https://doi.org/10.1253/circj.cj-08-0234

Wen B, Yuan H, Liu X, Wang H, Chen S, Chen Z et al (2017) GATA5 SUMOylation is indispensable for zebrafish cardiac development. Biochim Biophys Acta Gen Subj 1861:1691–1701. https://doi.org/10.1016/j.bbagen.2017.03.005

Willaert A, Khatri S, Callewaert BL, Coucke PJ, Crosby SD, Lee JG et al (2012) GLUT10 is required for the development of the cardiovascular system and the notochord and connects mitochondrial function to TGFβ signaling. Hum Mol Genet 21:1248–1259. https://doi.org/10.1093/hmg/ddr555

Yamase M, Nakazato Y, Daida H (2012) Effectiveness of amiodarone versus bepridil in achieving conversion to sinus rhythm in patients with persistent atrial fibrillation: a randomised trial. Heart 98:1067–1071. https://doi.org/10.1136/heartjnl-2012-302017

Yedinak KC (1993) Use of calcium channel antagonists for cardiovascular disease. Am Pharm NS33:49–64. https://doi.org/10.1016/s0160-3450(15)30720-0

Zeller FP, Spinler SA (1987) Bepridil: a new long-acting calcium channel blocking agent. Drug Intell Clin Pharm 21:487–492. https://doi.org/10.1177/106002808702100601